Distributed finite-time performance-prescribed time-varying formation control of autonomous surface vehicles with saturated inputs

Wentao Wu [a,b], Yibo Zhang [a], Weidong Zhang [a,c,*], Wei Xie [a,**]

[a] *Department of Automation, Shanghai Jiao Tong University, Shanghai 200240, China*
[b] *SJTU Sanya Yazhou Bay Institute of Deepsea Science and Technology, Sanya 572024, Hainan, China*
[c] *School of Information and Communication Engineering, Hainan University, Haikou 570228, Hainan, China*

ARTICLE INFO

ABSTRACT

This paper studies a time-varying formation control problem of a swarm of autonomous surface vehicles (ASVs) with prescribed constraints. Every ASV suffers from unavailable velocities, saturated inputs, internal uncertainties, and external disturbances. A distributed finite-time performance-prescribed time-varying formation control method is proposed for ASVs. Specifically, an adaptive fuzzy state observer (AFSO) is firstly proposed to recover the unavailable velocity by using saturated inputs and estimated disturbances from the fuzzy logic system. Secondly, a tunnel prescribed performance (TPP) function is designed to limit tracking errors with a concise form and smaller overshoot. At the kinematic level, with TPP-based error transformation, a C^1 finite-time time-varying guidance law is proposed by using the smooth switch functions and recovered velocities. Next, a finite-time command filter based on Levant differentiator is presented to smooth the guidance signals. At the kinetic level, a C^1 finite-time saturated control law is developed with the estimated velocities and disturbances. Then, it proves that tracking errors of the proposed closed-loop system converge into a small neighborhood around the equilibrium within finite time while evolving under TPP constraints regardless of saturated inputs. Finally, comparison results are provided to demonstrate the effectiveness of the proposed distributed finite-time performance-prescribed time-varying formation control method.

1. Introduction

In recent years, formation control of autonomous surface vehicles (ASVs) has fascinated considerable attention from both robotics and control communities due to various applications in military, commercial and civilian fields (Shi et al., 2017; Wu et al., 2022c,d; Zhang et al., 2021b,a; Yu et al., 2019; Du et al., 2022). According to Peng et al. (2021), existing formation control schemes include cooperative path following (Wu et al., 2022a; Peng et al., 2019), cooperative trajectory tracking (Jia et al., 2019; Park and Yoo, 2019), cooperative target tracking (Gao et al., 2022; Wu et al., 2022b). Among them, cooperative trajectory tracking is more challenging due to its spatial–temporal coupling characteristics, which can cause a worsened transient performance and a high possibility of actuator saturation.

Prescribed performance control (PPC) is an effective technique to improve transient and stable performance of controlled system. Up to now, lots of PPC-based formation control results for a swarm of ASVs have been developed in Dai et al. (2015, 2018), He et al. (2019),

Dai et al. (2022a,b), Chen et al. (2020), Jia et al. (2019), Lu et al. (2021), Wang et al. (2021a), Zhang and Chai (2021), Li et al. (2022a), Zhang and Yang (2018). Specifically, in Dai et al. (2015), a neural-learning-based control method with guaranteed transient performances is presented for marine vehicles without prior model dynamics. Based on PPC and dynamic surface control techniques, Dai et al. (2018) develops a platoon formation control scheme for multiple marine vessels, which is capable of achieving the platoons proceed along a given trajectory. In He et al. (2019), a decentralized leader–follower control strategy is proposed for the collision-free formation of multiple vessels. In Dai et al. (2022a), a formation tracking algorithm based on leader–follower architecture is devised, which is capable not only of guaranteeing the predefined transient properties but also of achieving connectivity maintenance and collision avoidance. In Dai et al. (2022b), a performance-guaranteed formation controller is presented by using the cooperative deterministic learning technique. In Chen et al. (2020), an adaptive trajectory tracking controller with predefined

---

transient performance is proposed for ASVs by using full-state feedback and output feedback schemes. In Jia et al. (2019) and Lu et al. (2021), adaptive performance-guaranteed formation control methods are developed for marine vessels. In Jia et al. (2019), the parameter compression technique is used to overcome persistent perturbations and model uncertainties in a more concise way. In Lu et al. (2021), two types of fault-tolerant kinetic controllers are presented for fault-based and fault-unknown scenarios. In Wang et al. (2021a), a performance function with flexible shape and appointed-time convergence is brought into the dynamic positioning control of vessels by combining with the event-triggered mechanism. In Zhang and Chai (2021), a non-singular adaptive trajectory tracking control scheme is presented by constructing an auxiliary variable. In Li et al. (2022a), a dedicated predefined performance dynamic positioning scheme is developed for marine vehicles with a robust adaptive neural network. In Zhang and Yang (2018), a low-complexity PPC method with the relaxed initial condition is proposed for multiple marine vessels with model uncertainties and actuator faults. Notice that although PPC methods in Dai et al. (2015, 2018), He et al. (2019), Dai et al. (2022a,b), Chen et al. (2020), Lu et al. (2021), Wang et al. (2021a), Zhang and Chai (2021), Li et al. (2022a) and Zhang and Yang (2018) achieve the formation control under prescribed constraints, but there are some points to be improved. Firstly, the tradition PPC constraint bounds are on either side of the origin, which still causes the overshoot problem of multi-ASV formation. Secondly, above methods rely on not only the position and heading information, but also the velocity signals. But some ASVs, especially for little and low-cost ones, are not capable of obtaining the velocity signals. Thirdly, above references do not consider the actuator saturation of ASVs, which may make prescribed constraints violated.

Motivated by above discussions, this paper develops a distributed finite-time performance-prescribed time-varying formation control method for a swarm of ASVs with unmeasurable velocities, saturated inputs, internal uncertainties, and external disturbances. Specifically, to recover unavailable velocities, an adaptive fuzzy state observer (AFSO) is firstly designed based on the estimated disturbances from fuzzy logic system (FLS) by using the position, heading, and saturated inputs. Next, a tunnel prescribed performance (TPP) function without the aid of initial values is constructed to limit the tracking errors in a concise manner. At the kinematic level, based on the TPP-transformed error systems, a C^1 distributed finite-time time-varying guidance law is proposed for ASVs by using recovered velocities. Then, a finite-time command filter based on Levant differentiator is presented to smooth the derivatives of guidance signals. At the kinetic level, a C^1 finite-time saturated control law is developed based on the anti-disturbance technique and the AFSO. It is proved that tracking errors of the closed-loop system converge into a small neighborhood around the equilibrium in finite time while obeying the TPP constraints. Finally, simulation results with comparison analysis are given for illustrating the effectiveness and advantages of the proposed method.

Compared with existing references, the main contributions of this paper are summarized into the following three-folds: 1) In contrast to the existing PPC methods in Dai et al. (2015, 2018), He et al. (2019), Dai et al. (2022a,b), Chen et al. (2020), Jia et al. (2019), Lu et al. (2021), Wang et al. (2021a), Zhang and Chai (2021), Li et al. (2022a), Park and Yoo (2019), Zhang and Yang (2018), Wang et al. (2021b) and Zhu et al. (2021), the TPP function with tight space is proposed to reduce the overshoot of multi-ASV formation system in a positive pattern. Besides, formation controller design and stability analysis do not depend on different initial errors. 2) In contrast to the state-feedback PPC methods (Dai et al., 2015, 2018; He et al., 2019; Dai et al., 2022a,b; Chen et al., 2020; Lu et al., 2021; Wang et al., 2021a; Zhang and Chai, 2021; Li et al., 2022a; Zhang and Yang, 2018) with prior velocity information, this paper presents an AFSO-based time-varying formation control method with prescribed performance by using the position and heading angle. Based on proposed control laws, the time-varying formation of ASVs with saturated inputs can be achieved while tracking errors satisfy the prescribed constraints. 3) In contrast to formation control methods in Dai et al. (2015, 2018), He et al. (2019), Dai et al. (2022a,b), Chen et al. (2020), Jia et al. (2019), Lu et al. (2021), Wang et al. (2021a), Zhang and Chai (2021), Li et al. (2022a), Park and Yoo (2019), Zhang and Yang (2018), Wang et al. (2021b) and Zhu et al. (2021), a finite-time prescribed time-varying formation control scheme is developed for multiple ASVs. Different from finite-time methods in Li et al. (2021, 2022b), Gu et al. (2019), Li et al. (2020) and Wang et al. (2019), the proposed C^1 finite-time guidance and control laws are no singularity by introducing piecewise functions of errors.

This paper is organized as follows. Section 2 introduces the preliminaries and problem formulation. Section 3 designs a distributed finite-time performance-prescribed time-varying formation control method. Section 4 analyzes the stability of the closed-loop system. Section 5 provides an application. Section 6 concludes this paper.

2. Preliminaries and problem formulation

2.1. Notations and lemmas

Throughout this paper, diag$\{\cdots\}$ presents a block-diagonal matrix. $|\cdot|$ and $\|\cdot\|$ are the absolute value of a real number and the Euclidean norm of a vector, respectively. $\bar{\lambda}(\cdot)$ and $\underline{\lambda}(\cdot)$ represent the minimum and maximum eigenvalues of a symmetric matrix. I_n represents an n-dimensional identity matrix. For $x = [x_1, \ldots, x_n]^T \in \mathfrak{R}^n$ and $0 < a < 1$, sig$^a(x)$ is defined as sig$^a(x) = [\text{sign}(x_1)|x_1|^a, \ldots, \text{sign}(x_n)|x_n|^a]^T$ with sign$(\cdot)$ being a signum function. Here, some necessary lemmas are introduced in this paper.

Lemma 1 (*Qian and Lin, 2001*).*Given any real number $x_i \in \mathfrak{R}, i = 1, \ldots, m$, and there is a positive constant $0 < q < 1$ such that*

$$\left(\sum_{i=1}^m |x_i| \right)^q \le \sum_{i=1}^m |x_i|^q. \tag{1}$$

Lemma 2 (*Qian and Lin, 2001*). *For two positive constants a, b, and a real-valued function $\chi(x, y) > 0$, the following inequality holds*

$$|x|^a |y|^b \le \frac{a\chi(x, y)}{a+b}|x|^{a+b} + \frac{b\chi^{-\frac{a}{b}}(x, y)}{a+b}|y|^{a+b}. \tag{2}$$

Lemma 3 (*Yu et al., 2005*). *Consider a nonlinear system $\dot{x} = f(x)$ with the initial state $x(t_0) = x_0 \in \mathfrak{R}^n$. For a positive-definite function $V(x)$, if there exists real constants $c > 0$, $d > 0$ and $0 < \beta < 1$ such that*

$$\dot{V}(x) \le -cV(x) - dV^\beta(x). \tag{3}$$

Then, the system is called to be finite-time stable, and the settling time satisfies $T = t_0 + 1/(c(1-\beta)) \times \ln((cV^{1-\beta}(x_0) + d)/d)$.

2.2. Fuzzy logic system

A FLS consists of four parts, i.e. a knowledge base, a fuzzy inference rule, a fuzzifier, and a defuzzifier. The knowledge base is composed of some "IF-THEN" rules as follows (Wang, 1994):

IF^l : If x_1 is $\mathcal{J}_1^l$, x_2 is $\mathcal{J}_2^l, \ldots,$ x_n is $\mathcal{J}_n^l$,

Then : y is $\mathcal{I}^l$, $l = 1, \ldots, m$,

where $x = [x_1, x_2, \ldots, x_n]^T \in \mathfrak{R}^n$ and y is the input and output of the FLS, respectively. m denotes the number of inference rules. The fuzzy sets of x_i and y are defined as $\mathcal{J}_i^l$ and $\mathcal{I}^l$ with corresponding membership functions expressed by $\mu_{\mathcal{J}_i^l}(x_i)$ and $\mu_{\mathcal{I}^l}(y)$, respectively. Then, the output $y(x)$ is defined as

$$y(x) = \frac{\sum_{l=1}^m W_l \prod_{i=1}^n \mu_{\mathcal{J}_i^l}(x_i)}{\sum_{l=1}^m \prod_{i=1}^n \mu_{\mathcal{J}_i^l}(x_i)},$$
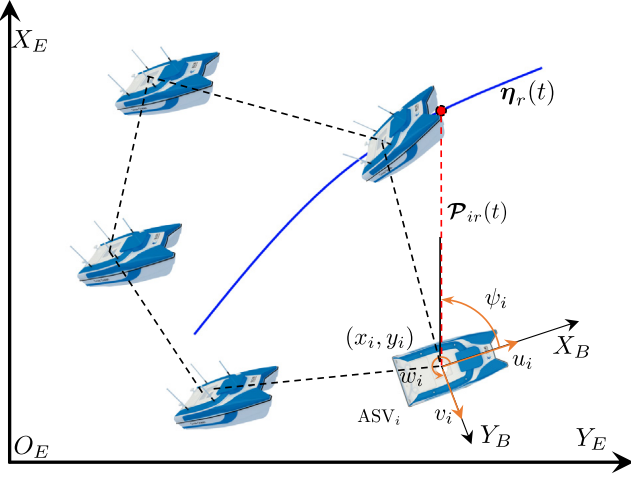
Fig. 1. The distributed formation pattern of N ASVs guided by one reference trajectory.

where $W_l = \max_{y \in R} \mu_{I^l}(y)$.

Letting $\boldsymbol{W} = [W_1, \ldots, W_m]^T$ and $\boldsymbol{\varphi}(\boldsymbol{x}) = [\varphi_1(\boldsymbol{x}), \varphi_2(\boldsymbol{x}), \ldots, \varphi_m(\boldsymbol{x})]^T$ with

$$\varphi_l(\boldsymbol{x}) = \frac{\prod_{i=1}^n \mu_{\mathcal{J}_i^l}(x_i)}{\sum_{l=1}^m \prod_{i=1}^n \mu_{\mathcal{J}_i^l}(x_i)},$$

the FLS can be written as $y(\boldsymbol{x}) = \boldsymbol{W}^T \boldsymbol{\varphi}(\boldsymbol{x})$.

Lemma 4 (*Wang, 1994*). *Given a continuous function $f(\boldsymbol{x})$ defined on a compact set Ω. There exists an FLS such that*

$$\sup_{\boldsymbol{x} \in \Omega} |f(\boldsymbol{x}) - \boldsymbol{W}^T \boldsymbol{\varphi}(\boldsymbol{x})| \leq \epsilon, \tag{4}$$

where $\epsilon \in \mathfrak{R}^+$.

2.3. Problem formulation

Consider a formation system containing N ASVs shown in Fig. 1. The motion of ASVs is usually described in the north-east reference frame denoted as $X_E - Y_E$ and the body-fixed reference frame denoted as $X_B - Y_B$. The kinematic and kinetic dynamics of the ith ASV are presented as follows (Fossen, 2011)

$$\begin{cases} \dot{\boldsymbol{\eta}}_i = \boldsymbol{R}(\psi_i)\boldsymbol{\vartheta}_i, \\ \boldsymbol{M}_i\dot{\boldsymbol{\vartheta}}_i = \boldsymbol{f}_i(\boldsymbol{\vartheta}_i) + \boldsymbol{\tau}_i + \boldsymbol{\tau}_{id}, \end{cases} \tag{5}$$

where $i = 1, \ldots, N$, $\boldsymbol{\eta}_i = [x_i, y_i, \psi_i]^T \in \mathfrak{R}^3$ is the only measurable position and the heading angle in $X_E - Y_E$. $\boldsymbol{\vartheta}_i = [u_i, v_i, w_i]^T \in \mathfrak{R}^3$ denotes the unavailable surge, sway, and yaw velocity vector in $X_B - Y_B$. $\boldsymbol{M}_i = \boldsymbol{M}_i^T \in \mathfrak{R}^{3 \times 3}$ is a inertia mass matrix. $\boldsymbol{f}_i(\boldsymbol{\vartheta}_i) \in \mathfrak{R}^3$ is an unknown uncertainty function vector including Coriolis terms, damping terms, and unmodeled dynamics. $\boldsymbol{\tau}_{id} \in \mathfrak{R}^3$ is the external disturbance term due to wind, wave and current. $\boldsymbol{\tau}_i \in \mathfrak{R}^3$ represents the actual control torques and moment expressed as $\tau_{il} = \mu_{il}(t, t_0)\tau_{is}^l$, $l = u, v, w$, where $\mu_{il}(t, t_0) \in [0, 1]$ and τ_{is}^l respectively represent an effectiveness function and the saturated term satisfying

$$\tau_{is}^l = \begin{cases} \bar{\tau}_{ia}^l, & \tau_{ia}^l \geq \bar{\tau}_{ia}^l, \\ \tau_{ia}^l, & \underline{\tau}_{ia}^l \leq \tau_{ia}^l \leq \bar{\tau}_{ia}^l, \\ \underline{\tau}_{ia}^l, & \tau_{ia}^l \geq \underline{\tau}_{ia}^l \end{cases} \tag{6}$$

with $\tau_{ia}^l \in \mathfrak{R}$ being the saturated control input, and $\bar{\tau}_{ia}^l \in \mathfrak{R}$ and $\underline{\tau}_{ia}^l \in \mathfrak{R}$ being assumed to be known upper and lower bounds. $\boldsymbol{R}(\psi_i)$ is a rotation matrix expressed as

$$\boldsymbol{R}_i = \begin{bmatrix} \cos(\psi_i) & -\sin(\psi_i) & 0 \\ \sin(\psi_i) & \cos(\psi_i) & 0 \\ 0 & 0 & 1 \end{bmatrix}.$$
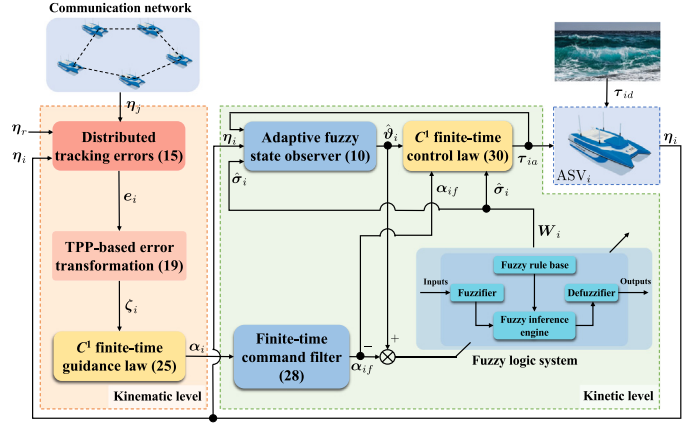

Fig. 2. The block diagram of the proposed controller for ASVs.

Consider a virtual leader moving along a predefined trajectory $\boldsymbol{\eta}_r(t) = [x_r(t), y_r(t), \psi_r(t)]^T \in \mathfrak{R}^3$ with $\psi_r(t) = \text{atan2}(\dot{y}_r(t), \dot{x}_r(t))$. To depict the communication relationship between the virtual leader and ASVs, a graph $\mathcal{G}$ is defined as $\mathcal{G} = \{\mathcal{V}, \mathcal{E}\}$, where $\mathcal{V}$ is a node set with $\mathcal{V} = \{\mathcal{V}^F, \mathcal{V}^L\}$ being the sets of ASVs and the virtual leader, and $\mathcal{E}$ is an edge set with $\mathcal{E} = \{(i, j) \in \mathcal{V} \times \mathcal{V}\}$. Define the neighborhood set $\mathcal{N}_i$ of the ith ASV as $\mathcal{N}_i = \{\mathcal{N}_i^F, \mathcal{N}_i^L\}$, where $\mathcal{N}_i^F = \{j \in \mathcal{V}_i^F | (i, j) \in \mathcal{E}\}$ and $\mathcal{N}_i^L = \{j \in \mathcal{V}_i^L | (i, j) \in \mathcal{E}\}$. The following assumptions are used in this paper.

Assumption 1. The derivative of the predefined trajectory $\boldsymbol{\eta}_r(t)$ is bounded and satisfied with $\|\dot{\boldsymbol{\eta}}_r\| \leq \bar{\eta}_r \in \mathfrak{R}^+$.

Assumption 2. The graph $\mathcal{G}$ contains a spanning tree with the virtual leader as the root node.

This paper aims to propose a distributed finite-time performance-prescribed time-varying formation control method for a swarm of ASVs such that: (1) To simplify the controller design, we develop a TPP with a concise form and smaller overshoot to limit the tracking error from violating specific constraints; (2) The proposed controller can force ASVs to track a predefined trajectory and hold a desired formation satisfying

$$\lim_{t \to T} \|\boldsymbol{\eta}_i(t) - \boldsymbol{\eta}_r(t) - \boldsymbol{\mathcal{P}}_{ir}(t)\| < \Delta_i, \tag{7}$$

in finite time, where T and Δ_i are some positive constants; $\boldsymbol{\mathcal{P}}_{ir}(t) \in \mathfrak{R}^3$ denotes a predefined time-varying deviation between the ith ASV and virtual leader.

3. Controller design

In this section, a distributed finite-time performance-prescribed time-varying formation control method for multiple ASVs is designed based on TPPs. And its block diagram is shown in Fig. 2.

3.1. Adaptive fuzzy state observer

In view of the excellent approximation properties of FLS to any unknown continuous functions, an AFSO is proposed before designing the formation controller. To simplify subsequent design, the kinetic equation of (5) is rewritten as

$$\dot{\boldsymbol{\vartheta}}_i = \boldsymbol{\sigma}_i + \boldsymbol{M}_i^{-1}\boldsymbol{\tau}_i \tag{8}$$

with $\boldsymbol{\sigma}_i = \boldsymbol{M}_i^{-1}(\boldsymbol{f}_i(\boldsymbol{\vartheta}_i) + \boldsymbol{\tau}_{id})$, which can be approximated by the following adaptive FLS

$$\hat{\boldsymbol{\sigma}}_i(\hat{\boldsymbol{\vartheta}}_i | \boldsymbol{W}_i) = \boldsymbol{W}_i^T \boldsymbol{\varphi}_i(\hat{\boldsymbol{\vartheta}}_i),$$
$$\boldsymbol{W}_i^* = \arg\min_{\boldsymbol{W}_i}[\sup \|\boldsymbol{W}_i^T \boldsymbol{\varphi}_i(\hat{\boldsymbol{\vartheta}}_i) - \boldsymbol{\sigma}_i\|], \tag{9}$$

where $\hat{\sigma}_i(\hat{\vartheta}_i|W_i) \in \Re^3$ presents the estimation of σ_i; $\varphi_i(\hat{\vartheta}_i) \in \Re^{3m}$ is the fuzzy basis function with the estimated value $\hat{\vartheta}_i \in \Re^3$; $W_i^* \in \Re^{3m\times3}$ is the optimal fuzzy weight matrix and $W_i \in \Re^{3m\times3}$ denotes the estimation of W_i^*.

Let $\hat{\eta}_i = [\hat{x}_i, \hat{y}_i, \hat{\psi}_i]^T \in \Re^3$ be the estimated vector of η_i. According to (5), (8) and (9), the AFSO is designed as follow

$$\begin{cases} \dot{\hat{\eta}}_i = -L_{i1}(\hat{\eta}_i - \eta_i) + R_i\hat{\vartheta}_i, \\ \dot{\hat{\vartheta}}_i = -L_{i2}R_i^T(\hat{\eta}_i - \eta_i) + \hat{\sigma}_i + M_i^{-1}\tau_{is}, \end{cases} \tag{10}$$

where $L_{i1} \in \Re^{3\times3}$ and $L_{i2} \in \Re^{3\times3}$ are positive gain matrices.

Based on the online data from (10), a adaptive law is developed as follows

$$\dot{W}_i = -\varsigma_i\left(\varphi_i\vartheta_{ie}^T + \xi_i W_i\right), \tag{11}$$

where $\varsigma_i = \mathrm{diag}\{\varsigma_{iu}I_m, \varsigma_{iv}I_m, \varsigma_{iw}I_m\}$ and $\xi_i = \mathrm{diag}\{\xi_{iu}I_m, \xi_{iv}I_m, \xi_{iw}I_m\}$ with $\varsigma_{iu}, \varsigma_{iv}, \varsigma_{iw}, \xi_{iu}, \xi_{iv}$ and ξ_{iw} being positive constants. ϑ_{ie} will be given in the next subsection.

Define observer errors as $\tilde{\eta}_i = \hat{\eta}_i - \eta_i$ and $\tilde{\vartheta}_i = \hat{\vartheta}_i - \vartheta_i$. With the Eqs. (5), (8) and (10), the error dynamics can be written as follows

$$\begin{cases} \dot{\tilde{\eta}}_i = -L_{i1}\tilde{\eta}_i + R_i\tilde{\vartheta}_i, \\ \dot{\tilde{\vartheta}}_i = -L_{i2}R_i^T\tilde{\eta}_i + \hat{\sigma}_i - \sigma_i + M_i^{-1}(\tau_{is} - \tau_i). \end{cases} \tag{12}$$

Letting $E_i = [\tilde{\eta}_i^T, \tilde{\vartheta}_i^T]^T$, it takes the derivative of E_i along (12) as follows

$$\dot{E}_i = A_i E_i + B_i\left(\hat{\sigma}_i - \sigma_i + M_i^{-1}(\tau_{is} - \tau_i)\right), \tag{13}$$

where $A_i = \begin{bmatrix} -L_{i1} & R_i \\ -L_{i2}R_i^T & 0_3 \end{bmatrix}$ and $B_i = \begin{bmatrix} 0_3 \\ I_3 \end{bmatrix}$.

Obviously, A_i is a Hurwitz matrix. Then, there exists a positive definite matrix $P_i \in \Re^{6\times6}$ such that

$$A_i^T P_i + P_i A_i = -Q_i \tag{14}$$

with $Q_i \in \Re^{6\times6}$ being a positive definite matrix.

3.2. Controller design

In the above subsection, the proposed AFSO is used to recover the unknown velocities. This subsection presents the kinematic guidance laws and the kinetic control laws.

3.2.1. Kinematic level

To achieve the distributed time-varying formation of multiple ASVs guided by the virtual leader, an earth-fixed distributed tracking error $e_i = [e_{ix}, e_{iy}, e_{i\psi}]^T$ is defined as follows

$$e_i = \sum_{j\in\mathcal{N}_i^F} a_{ij}(\eta_i - \eta_j - \mathcal{P}_{ij}) + a_{i0}(\eta_i - \eta_r - \mathcal{P}_{ir}), \tag{15}$$

where $\mathcal{P}_{ij} = \mathcal{P}_{ir} - \mathcal{P}_{jr}$. If the ith ASV can receive the position and heading information of the jth ASV, $a_{ij} = 1$; otherwise, $a_{ij} = 0$. If the ith ASV can receive the information of the virtual leader, $a_{i0} = 1$; otherwise, $a_{i0} = 0$.

From the kinematics (5), the derivative of e_i is deduced as

$$\dot{e}_i = d_i R_i\vartheta_i - \sum_{j\in\mathcal{N}_i^F} a_{ij}R_j\vartheta_j - a_{i0}\dot{\eta}_r - \sum_{j\in\mathcal{N}_i} a_{ij}\dot{\mathcal{P}}_{ij}, \tag{16}$$

where $d_i = \sum_{j\in\mathcal{N}_i^F} a_{ij} + a_{i0}$.

In order to improve the transient and steady-state performance of multi-ASV formation, the tracking errors are forced to satisfy the following TPP constraints

$$-\underline{e}_{ik}(t) \leq e_{ik}(t) \leq \bar{e}_{ik}(t), \quad k = x, y, \psi, \tag{17}$$

where $\bar{e}_{ik}(t)$ and $\underline{e}_{ik}(t)$ are the time-varying functions defined as

$$\begin{cases} \bar{e}_{ik} = \left(\bar{\delta}_{ik} + \mathrm{sig}(e_{ik,0})\right)\rho_{ik}(t) - \rho_{ik,\infty}\mathrm{sig}(e_{ik,0}), \\ \underline{e}_{ik} = \left(\underline{\delta}_{ik} - \mathrm{sig}(e_{ik,0})\right)\rho_{ik}(t) + \rho_{ik,\infty}\mathrm{sig}(e_{ik,0}) \end{cases} \tag{18}$$

with $0 \leq \bar{\delta}_{ik}, \underline{\delta}_{ik} \leq 1$. $\rho_{ik}(t) = (\rho_{ik,0} - \rho_{ik,\infty})\exp(-\varkappa_{ik}t) + \rho_{ik,\infty}$, where $\rho_{ik,0} = \rho_{ik}(0)$, $\rho_{ik,\infty} = \lim_{t\to\infty}\rho_{ik}(t)$, $\rho_{ik,0} > \rho_{ik,\infty} > 0$, and $\varkappa_{ik} \in \Re^+$.

Next, we construct an error transformation function as follows

$$e_{ik}(t) = \frac{\bar{e}_{ik}(t) + \underline{e}_{ik}(t)}{2}Y_{ik}(\zeta_{ik}) + \frac{\bar{e}_{ik}(t) - \underline{e}_{ik}(t)}{2}, \tag{19}$$

where $Y_{ik}(\zeta_{ik}) : (-\infty, \infty) \mapsto (-1, 1)$ is a smooth and strictly increasing transformation function with ζ_{ik} being an unconstrained variable equivalent to $e_{ik}(t)$. Here, the transformation function $Y_{ik}(\zeta_{ik})$ is selected as $Y_{ik}(\zeta_{ik}) = (\exp(\zeta_{ik}) - \exp(-\zeta_{ik}))/(\exp(\zeta_{ik}) + \exp(-\zeta_{ik}))$. By solving the inverse function of $Y_{ik}(\zeta_{ik})$, the transformed error ζ_{ik} is deduced as follows

$$\zeta_{ik} = Y_{ik}^{-\mathrm{inv}}(e_{ik}, \bar{e}_{ik}, \underline{e}_{ik}) = \ln\frac{1 + Y_{ik}}{1 - Y_{ik}}, \tag{20}$$

where $Y_{ik} = (2e_{ik} - \bar{e}_{ik} + \underline{e}_{ik})/(\bar{e}_{ik} + \underline{e}_{ik})$. Taking the time derivative of ζ_{ik} yields as follows

$$\dot{\zeta}_{ik} = \frac{\partial\zeta_{ik}}{\partial Y_{ik}}\left(\frac{\partial Y_{ik}}{\partial e_{ik}}\dot{e}_{ik} + \frac{\partial Y_{ik}}{\partial\bar{e}_{ik}}\dot{\bar{e}}_{ik} + \frac{\partial Y_{ik}}{\partial\underline{e}_{ik}}\dot{\underline{e}}_{ik}\right), \tag{21}$$

where $\partial\zeta_{ik}/\partial Y_{ik} = 2/(1 - Y_{ik}^2)$, $\partial Y_{ik}/\partial e_{ik} = 2/(\bar{e}_{ik} + \underline{e}_{ik})$, $\partial Y_{ik}/\partial\bar{e}_{ik} = -2(\underline{e}_{ik} + e_{ik})/(\bar{e}_{ik} + \underline{e}_{ik})^2$, and $\partial Y_{ik}/\partial\underline{e}_{ik} = 2(\bar{e}_{ik} - e_{ik})/(\bar{e}_{ik} + \underline{e}_{ik})^2$.

Define the vectors $\zeta_i = [\zeta_{ix}, \zeta_{iy}, \zeta_{i\psi}]^T$, $\bar{e}_i = [\bar{e}_{ix}, \bar{e}_{iy}, \bar{e}_{i\psi}]^T$, and $\underline{e}_i = [\underline{e}_{ix}, \underline{e}_{iy}, \underline{e}_{i\psi}]^T$. Then, the error dynamics (21) is unified as the following form

$$\dot{\zeta}_i = \mathcal{F}_{e_i}\dot{e}_i + \mathcal{F}_{\bar{e}_i}\dot{\bar{e}}_i + \mathcal{F}_{\underline{e}_i}\dot{\underline{e}}_i, \tag{22}$$

where $\mathcal{F}_{e_i} = \mathrm{diag}\{\mathcal{F}_{e_{ik}}\} \in \Re^{3\times3}$ with $\mathcal{F}_{e_{ik}} = \partial\zeta_{ik}/\partial Y_{ik} \times \partial Y_{ik}/\partial e_{ik}$; $\mathcal{F}_{\bar{e}_i} = \mathrm{diag}\{\mathcal{F}_{\bar{e}_{ik}}\} \in \Re^{3\times3}$ with $\mathcal{F}_{\bar{e}_{ik}} = \partial\zeta_{ik}/\partial Y_{ik} \times \partial Y_{ik}/\partial\bar{e}_{ik}$; $\mathcal{F}_{\underline{e}_i} = \mathrm{diag}\{\mathcal{F}_{\underline{e}_{ik}}\} \in \Re^{3\times3}$ with $\mathcal{F}_{\underline{e}_{ik}} = \partial\zeta_{ik}/\partial Y_{ik} \times \partial Y_{ik}/\partial\underline{e}_{ik}$.

Substituting (16) into (22), one has

$$\begin{aligned} \dot{\zeta}_i = \mathcal{F}_{e_i}&\left(d_i R_i\vartheta_i - \sum_{j\in\mathcal{N}_i^F} a_{ij}R_j\vartheta_j - \sum_{j\in\mathcal{N}_i} a_{ij}\dot{\mathcal{P}}_{ij} - a_{i0}\dot{\eta}_r\right) \\ &+ \mathcal{F}_{\bar{e}_i}\dot{\bar{e}}_i + \mathcal{F}_{\underline{e}_i}\dot{\underline{e}}_i. \end{aligned} \tag{23}$$

Define errors $\vartheta_{ie} = \hat{\vartheta}_i - \alpha_{if}$ and $\alpha_{ie} = \alpha_{if} - \alpha_i$, where $\alpha_{if} \in \Re^3$ is the output of the command filter to be designed later. Substituting ϑ_{ie} and α_{ie} into (23) yields

$$\begin{aligned} \dot{\zeta}_i = \mathcal{F}_{e_i}&\left(d_i R_i(\alpha_i - \tilde{\vartheta}_i + \vartheta_{ie} + \alpha_{ie}) - \sum_{j\in\mathcal{N}_i} a_{ij}\dot{\mathcal{P}}_{ij} - a_{i0}\dot{\eta}_r\right. \\ &\left. - \sum_{j\in\mathcal{N}_i^F} a_{ij}R_j\vartheta_j\right) + \mathcal{F}_{\bar{e}_i}\dot{\bar{e}}_i + \mathcal{F}_{\underline{e}_i}\dot{\underline{e}}_i. \end{aligned} \tag{24}$$

To stabilize error dynamics in (24), a C^1 finite-time guidance law is proposed as

$$\begin{aligned} \alpha_i = \frac{R_i^T}{d_i}&\left(-\mathcal{F}_{e_i}^{-1}\left(K_{i1}\zeta_i + K_{i2}\gamma_i(\zeta_i) + \mathcal{F}_{\bar{e}_i}\dot{\bar{e}}_i + \mathcal{F}_{\underline{e}_i}\dot{\underline{e}}_i\right)\right. \\ &\left. + \sum_{j\in\mathcal{N}_i^F} a_{ij}R_j\hat{\vartheta}_j + \sum_{j\in\mathcal{N}_i} a_{ij}\dot{\mathcal{P}}_{ij} + a_{i0}\dot{\eta}_r\right), \end{aligned} \tag{25}$$

where $K_{i1} \in \Re^{3\times3}$ and $K_{i2} \in \Re^{3\times3}$ are the positive diagonal matrices. $\gamma_i(\zeta_i) = [\gamma_{ix}(\zeta_{ix}), \gamma_{iy}(\zeta_{iy}), \gamma_{i\psi}(\zeta_{i\psi})]^T$ with $\gamma_{ik}(\zeta_{ik})$ being smooth switching function defined as

$$\gamma_{ik}(\zeta_{ik}) = \begin{cases} \mathrm{sig}^{\beta_{i1}}(\zeta_{ik}), & |\zeta_{ik}| \geq \iota_{ik}, \\ \iota_{ik}^{\beta_{i1}-1}\zeta_{ik}, & |\zeta_{ik}| < \iota_{ik}, \end{cases} \tag{26}$$

where $0 < \beta_{i1} < 1$ and $\iota_{ik} \in \Re^+$.

Remark 1. In Gu et al. (2019), Ji et al. (2021) and Li et al. (2018), the proposed finite-time virtual control laws belong to the C^0 function, which means that the derivative of virtual control law is discontinuous. Compared with the C^0 control laws, the constructed function $\gamma_i(\zeta_i)$

can ensure that the finite-time guidance law (25) is continuous and differentiable. From (26), it can obtain that $\gamma_{ik}(\zeta_{ik}^+) = \lim_{\zeta_{ik} \to \iota_{ik}^+} = |\zeta_{ik}|^{\beta_{i1}}$ and $\gamma_{ik}(\zeta_{ik}^-) = \lim_{\zeta_{ik} \to \iota_{ik}^-} = |\zeta_{ik}|^{\beta_{i1}}$ when $\zeta_{ik} > 0$. Thus, one has $\gamma_{ik}(\iota_{ik}^+) = \gamma_{ik}(\iota_{ik}^-)$. Similarly, we have $\gamma_{ik}(-\iota_{ik}^+) = \gamma_{ik}(-\iota_{ik}^-)$ for $\zeta_{ik} < 0$. Hence, the continuity of $\gamma_{ik}(\zeta_{ik})$ can be satisfied. Taking the time derivative of $\gamma_{ik}(\zeta_{ik})$, it can devise that $\dot{\gamma}_{ik}(\iota_{ik}^+) = \dot{\gamma}_{ik}(\iota_{ik}^-)$ and $\dot{\gamma}_{ik}(-\iota_{ik}^+) = \dot{\gamma}_{ik}(-\iota_{ik}^-)$, which means that $\dot{\gamma}_{ik}(\zeta_{ik})$ is continuous.

Substituting (25) into (24), the transformed error dynamics are described as

$$\dot{\zeta}_i = \mathcal{F}_{e_i}\left(d_i R_i(-\tilde{\vartheta}_i + \vartheta_{ie} + \alpha_{ie}) + \sum_{j \in \mathcal{N}_i^F} a_{ij} R_j \tilde{\vartheta}_j \right)$$
$$- K_{i1}\zeta_i - K_{i2}\gamma_i(\zeta_i). \tag{27}$$

3.2.2. Kinetic level

For the sake of integrating the kinematic level and kinetic level, the guidance signal α_i is forced to pass a command filter. In order to improve the convergence speed and tracking accuracy, a finite-time command filter based on Levant differentiator is designed as follows (Levant, 1998)

$$\begin{cases} \dot{\alpha}_{if} = \alpha_{ic}, \\ \alpha_{ic} = -L_{i3}\text{sig}^{\frac{1}{2}}(\alpha_{if} - \alpha_i) + \alpha_{if}^d, \\ \dot{\alpha}_{if}^d = -L_{i4}\text{sig}^0(\alpha_{if}^d - \alpha_{ic}), \end{cases} \tag{28}$$

where $\alpha_{if} \in \mathfrak{R}^3$ and $\alpha_{if}^d \in \mathfrak{R}^3$ represent the filtered signals of α_i and the derivative of α_{if}, respectively. $\alpha_{ic} \in \mathfrak{R}^3$ is an intermediate variable. $L_{i3} \in \mathfrak{R}^{3\times3}$ and $L_{i4} \in \mathfrak{R}^{3\times3}$ are the positive diagonal coefficient matrices.

For the command filter (28), the input signal α_i is differentiable with $\|\alpha_i - \alpha_{i0}\| \leq \bar{\alpha}_{i0} \in \mathfrak{R}^+$, where α_{i0} is the input part without noise. According to the stability conclusion in Levant (1998), the command filter (28) is finite-time stable and satisfying $\|\alpha_{if} - \alpha_i\| \leq \bar{\alpha}_i \in \mathfrak{R}^+$ and $\|\alpha_{if}^d - \dot{\alpha}_i\| \leq \bar{\alpha}_i^d \in \mathfrak{R}^+$.

Along (10) and (28), it takes the time derivative of ϑ_{ie} as

$$\dot{\vartheta}_{ie} = -L_{i2}R_i^T\tilde{\eta}_i + \hat{\sigma}_i + M_i^{-1}\tau_{is} - \alpha_{if}^d. \tag{29}$$

Based on the estimated total disturbances from (9) and the filtered signal from (28), a C^1 finite-time saturated control law is designed as follows

$$\tau_{ia} = M_i\left(-K_{i3}\vartheta_{ie} - K_{i4}\gamma_i(\vartheta_{ie}) + L_{i2}R_i^T\tilde{\eta}_i + \alpha_{if}^d \right.$$
$$\left. - d_i R_i^T \mathcal{F}_{e_i}^T \zeta_i - \hat{\sigma}_i \right), \tag{30}$$

where $K_{i3} \in \mathfrak{R}^{3\times3}$ and $K_{i4} \in \mathfrak{R}^{3\times3}$ are the positive gain matrices. The switching function $\gamma_i(\vartheta_{ie}) = [\gamma_{iu}(\vartheta_{ie}^u), \gamma_{iv}(\vartheta_{ie}^v), \gamma_{iw}(\vartheta_{ie}^w)]^T$ is expressed as

$$\gamma_{il}(\vartheta_{ie}^l) = \begin{cases} \text{sig}^{\beta_{i2}}(\vartheta_{ie}^l), & |\vartheta_{ie}^l| \geq \iota_{il}, \\ \iota_{ie}^{\beta_{i2}-1}\vartheta_{ie}^l, & |\vartheta_{ie}^l| < \iota_{il}, \quad l = u, v, w, \end{cases} \tag{31}$$

where $0 < \beta_{i2} < 1$ and $\iota_{il} \in \mathfrak{R}^+$.

Substituting (30) into (29), the error dynamics is yielded as

$$\dot{\vartheta}_{ie} = -K_{i3}\vartheta_{ie} - K_{i4}\gamma_i(\vartheta_{ie}) - d_i R_i^T \mathcal{F}_{e_i}^T \zeta_i. \tag{32}$$

4. Main results

In the above section, the detailed design of the proposed distributed finite-time performance-prescribed time-varying formation method has been given. In this section, the main results are provided by the following theorem.

Theorem 1. *Consider a formation consisting of multiple ASVs with model dynamics* (5), *the saturated inputs* (6), *the AFSO* (10), *the adaptive law* (11), *the C^1 finite-time guidance law* (25), *the finite-time command filter* (28), *and the C^1 finite-time saturated control law* (30). *If Assumptions* 1

and 2 *are satisfied, tracking errors of the proposed closed-loop system converge to a small neighborhood around the equilibrium within finite time while not violating the TPP-based constraints regardless of saturated inputs.*

Proof. *Step 1:* Consider a Lyapunov function candidate $V_{i0} = E_i^T P_i E_i/2$ and take its time derivative of V_{i0} as

$$\dot{V}_{i0} = \frac{1}{2}E_i^T(A_i^T P_i + P_i A_i)E_i + E_i^T P_i B_i(\hat{\sigma}_i - \sigma_i)$$
$$+ E_i^T P_i B_i M_i^{-1}(\tau_{is} - \tau_i). \tag{33}$$

Because of $\tau_i = \mu_i(t, t_0)\tau_{is}$ and $\sigma_i = W_i^{*T}\varphi_i(\vartheta_i) + \epsilon_i$ with ϵ_i being the approximated error, combining (9), (14) and (33) renders that

$$\dot{V}_{i0} \leq -\frac{1}{2}E_i^T Q_i E_i + (1 - \mu_i)E_i^T P_i B_i M_i^{-1}\tau_{is}$$
$$- E_i^T P_i B_i\left(\tilde{W}_i^T\varphi_i(\hat{\vartheta}_i) + W_i^{*T}(\varphi_i(\vartheta_i) - \varphi_i(\hat{\vartheta}_i)) + \epsilon_i \right), \tag{34}$$

where $\tilde{W}_i = W_i^* - \hat{W}_i$.

Since W_{il}^*, $\varphi_{il}(l_i)$ and $\varphi_{il}(\hat{l}_i)$ are bounded, there exist constants $\varrho_1 \in \mathfrak{R}^+$, $\varrho_2 \in \mathfrak{R}^+$ such that $\|\varphi_i(\hat{\vartheta}_i)\| \leq \varrho_1$ and $\|W_i^{*T}(\varphi_i(\vartheta_i) - \varphi_i(\hat{\vartheta}_i)) + \epsilon_i\| \leq \varrho_2$. From the Young's inequality, one has $-E_i^T P_i B_i(\tilde{W}_i^T\varphi_i(\hat{\vartheta}_i) + W_i^{*T}(\varphi_i(\vartheta_i) - \varphi_i(\hat{\vartheta}_i)) + \epsilon_i) \leq \|E_i\|^2 + \|P_i\|^2(\varrho_1\|\tilde{W}_i\|^2 + \varrho_2^2)/2$ and $(1 - \mu_i)E_i^T P_i B_i M_i^{-1}\tau_{is} \leq \|E_i\|^2 + (1 - \mu_i)\|P_i\|^2\|M_i^{-1}\|^2\|\tau_{is}\|^2/2$. Then, (34) is further put into

$$\dot{V}_{i0} \leq -c_{i0}\|E_i\|^2 + \frac{\varrho_1}{2}\|P_i\|^2\|\tilde{W}_i\|^2 + \varepsilon_{i0}, \tag{35}$$

where $c_{i0} = (\underline{\lambda}(Q_i) - 4)/2$ and $\varepsilon_{i0} = \|P_i\|^2(\varrho_2^2 + (1 - \mu_i)\|M_i^{-1}\|^2\|\tau_{is}\|^2)/2$.

Step 2: Construct a Lyapunov function candidate as $V_{i1} = \zeta_i^T\zeta_i/2$.

From (27), it takes the time derivative of V_{i1} as

$$\dot{V}_{i1} = \zeta_i^T\mathcal{F}_{e_i}\left(d_i R_i(-\tilde{\vartheta}_i + \alpha_{ie}) + \sum_{j \in \mathcal{N}_i^F} a_{ij} R_j \tilde{\vartheta}_j \right)$$
$$+ d_i\zeta_i^T\mathcal{F}_{e_i}R_i\vartheta_{ie} - \zeta_i^T\left(K_{i1}\zeta_i + K_{i2}\gamma_i(\zeta_i) \right). \tag{36}$$

By utilizing Young's inequality, it gets $\zeta_i^T\mathcal{F}_{e_i}R_i(-\tilde{\vartheta}_i + \alpha_{ie}) \leq \|\zeta_i\|^2 + \|\mathcal{F}_{e_i}\|^2(\|\tilde{\vartheta}_i\|^2 + \|\alpha_{ie}\|^2)/2$ and $\zeta_i^T\mathcal{F}_{e_i}\sum_{j \in \mathcal{N}_i^F} a_{ij}R_j\tilde{\vartheta}_j \leq \sum_{j \in \mathcal{N}_i^F} a_{ij}\|\zeta_i\|^2/2 + \|\mathcal{F}_{e_i}\|^2\sum_{j \in \mathcal{N}_i^F} a_{ij}\|\tilde{\vartheta}_j\|^2/2$. Since $\|\alpha_{ie}\| \leq \bar{\alpha}_i$, it yields that $\dot{V}_{i1}$ meets

$$\dot{V}_{i1} \leq -\underline{\lambda}(K_{i1})\|\zeta_i\|^2 - \underline{\lambda}(K_{i2})\zeta_i^T\gamma_i(\zeta_i) + d_i\|\zeta_i\|^2$$
$$+ \frac{d_i}{2}\|\mathcal{F}_{e_i}\|^2\left(\|\tilde{\vartheta}_i\|^2 + \bar{\alpha}_i^2 \right) + d_i\zeta_i^T\mathcal{F}_{e_i}R_i\vartheta_{ie}$$
$$+ \frac{1}{2}\sum_{j \in \mathcal{N}_i^F} a_{ij}\|\zeta_i\|^2 + \frac{1}{2}\|\mathcal{F}_{e_i}\|^2\sum_{j \in \mathcal{N}_i^F} a_{ij}\|\tilde{\vartheta}_j\|^2. \tag{37}$$

Letting $c_{i1} = \underline{\lambda}(K_{i1}) - d_i - \frac{1}{2}\sum_{j \in \mathcal{N}_i^F} a_{ij}$ and $c_{i2} = \underline{\lambda}(K_{i2})$, the time derivative of V_{i1} can be presented as

$$\dot{V}_{i1} \leq -c_{i1}\|\zeta_i\|^2 - c_{i2}\zeta_i^T\gamma_i(\zeta_i) + d_i\zeta_i^T\mathcal{F}_{e_i}R_i\vartheta_{ie}$$
$$+ \frac{1}{2}\|\mathcal{F}_{e_i}\|^2\left(d_i\|\tilde{\vartheta}_i\|^2 + \sum_{j \in \mathcal{N}_i^F} a_{ij}\|\tilde{\vartheta}_j\|^2 \right) + \varepsilon_{i1}, \tag{38}$$

where $\varepsilon_{i1} = d_i\bar{\alpha}_i^2\|\mathcal{F}_{e_i}\|^2/2$.

Step 3: Design a Lyapunov function candidate as

$$V_{i2} = \frac{1}{2}\vartheta_{ie}^T\vartheta_{ie} + \frac{1}{2}\tilde{W}_i^T\varsigma_i^{-1}\tilde{W}_i. \tag{39}$$

Differentiating V_{i2} along the dynamics (11) and (32), it gets

$$\dot{V}_{i2} = -\vartheta_{ie}^T(K_{i3}\vartheta_{ie} + K_{i4}\gamma_i(\vartheta_{ie}) + d_i R_i^T\mathcal{F}_{e_i}^T\zeta_i)$$
$$+ \tilde{W}_i^T(\varphi_i(\hat{\vartheta}_i)\vartheta_{ie}^T + \xi_i W_i). \tag{40}$$

Using Young's inequality and $0 \leq \varphi_{il}(\hat{l}_i) \leq 1$, we have

$$\tilde{W}_i^T\varphi_i(\hat{\vartheta}_i)\vartheta_{ie}^T \leq \frac{1}{2}\|\tilde{W}_i\|^2 + \frac{1}{2}\|\vartheta_{ie}\|^2,$$
$$\tilde{W}_i^T\xi_i W_i \leq -\frac{1}{2}\bar{\lambda}(\xi_i)\|\tilde{W}_i\|^2 + \frac{1}{2}\bar{\lambda}(\xi_i)\|W_i^*\|^2. \tag{41}$$

Taking (41) into (40), $\dot{V}_{i2}$ is rewritten as follows

$$
\begin{aligned}
\dot{V}_{i2} \le & -\underline{\lambda}(\boldsymbol{K}_{i3})\|\boldsymbol{\vartheta}_{ie}\|^2 - \underline{\lambda}(\boldsymbol{K}_{i4})\boldsymbol{\vartheta}_{ie}^T\boldsymbol{\gamma}_i(\boldsymbol{\vartheta}_{ie}) + \frac{1}{2}\Big(\ \|\tilde{\boldsymbol{W}}_i\|^2 + \\
& \|\boldsymbol{\vartheta}_{ie}\|^2 - \bar{\lambda}(\xi_i)\|\tilde{\boldsymbol{W}}_i\|^2 + \bar{\lambda}(\xi_i)\|\boldsymbol{W}_i^*\|^2\ \Big) - d_i\boldsymbol{\vartheta}_{ie}^T\boldsymbol{R}_i^T\boldsymbol{\mathcal{F}}_{e_i}^T\boldsymbol{\zeta}_i \\
\le & -c_{i3}\|\boldsymbol{\vartheta}_{ie}\|^2 - c_{i4}\boldsymbol{\vartheta}_{ie}^T\boldsymbol{\gamma}_i(\boldsymbol{\vartheta}_{ie}) - c_{i5}\|\tilde{\boldsymbol{W}}_i\|^2 \\
& - d_i\boldsymbol{\vartheta}_{ie}^T\boldsymbol{R}_i^T\boldsymbol{\mathcal{F}}_{e_i}^T\boldsymbol{\zeta}_i + \varepsilon_{i2},
\end{aligned}
\tag{42}
$$

where $c_{i3} = \underline{\lambda}(\boldsymbol{K}_{i3}) - 1/2$, $c_{i4} = \underline{\lambda}(\boldsymbol{K}_{i4})$, $c_{i5} = (\bar{\lambda}(\xi_i) - 1)/2$ and $\varepsilon_{i2} = \bar{\lambda}(\xi_i)\|\boldsymbol{W}_i^*\|^2/2$.

Step 4: Consider the following Lyapunov function candidate

$$
V = \sum_{i=1}^N (V_{i0} + V_{i1} + V_{i2}).
\tag{43}
$$

From inequalities (35), (38) and (42), it takes the time derivative of V as follows

$$
\begin{aligned}
\dot{V} \le \sum_{i=1}^N \Big(& -c_{i0}'\|\boldsymbol{E}_i\|^2 - c_{i1}\|\boldsymbol{\zeta}_i\|^2 - c_{i2}\boldsymbol{\zeta}_i^T\boldsymbol{\gamma}_i(\boldsymbol{\zeta}_i) - c_{i3}\|\boldsymbol{\vartheta}_{ie}\|^2 \\
& - c_{i4}\boldsymbol{\vartheta}_{ie}^T\boldsymbol{\gamma}_i(\boldsymbol{\vartheta}_{ie}) - c_{i5}'\|\tilde{\boldsymbol{W}}_i\|^2 + \varepsilon_i\ \Big).
\end{aligned}
\tag{44}
$$

where $c_{i0}' = c_{i0} - d_i\|\boldsymbol{\mathcal{F}}_{e_i}\|^2/2$, $c_{i5}' = c_{i5} - \|\boldsymbol{P}_i\|^2/2$, and $\varepsilon_i = \varepsilon_{i0} + \varepsilon_{i1} + \varepsilon_{i2} + \|\boldsymbol{\mathcal{F}}_{e_i}\|^2\sum_{j\in\mathcal{N}_i^F} a_{ij}\|\tilde{\boldsymbol{\vartheta}}_j\|^2$.

According to definitions of $\boldsymbol{\gamma}_i(\boldsymbol{\zeta}_i)$ and $\boldsymbol{\gamma}_i(\boldsymbol{\vartheta}_{ie})$, the stability of the closed-loop system is discussed by the following two cases.

Case 1. For $|\zeta_{ik}| < \iota_{ik}$ and $|\vartheta_{ie}^l| < \iota_{il}$, $i = 1, \ldots, N, k = x, y, \psi, l = u, v, w$, we have

$$
\boldsymbol{\gamma}_i(\boldsymbol{\zeta}_i) = \boldsymbol{\iota}_{i\zeta}\boldsymbol{\zeta}_i \quad \text{and} \quad \boldsymbol{\gamma}_i(\boldsymbol{\vartheta}_{ie}) = \boldsymbol{\iota}_{i\vartheta}\boldsymbol{\vartheta}_{ie},
\tag{45}
$$

where $\boldsymbol{\iota}_{i\zeta} = \text{diag}\{\zeta_{ix}^{\beta_{i1}-1}, \zeta_{iy}^{\beta_{i1}-1}, \zeta_{i\psi}^{\beta_{i1}-1}\}$ and $\boldsymbol{\iota}_{i\vartheta} = \text{diag}\{(\vartheta_{ie}^u)^{\beta_{i2}-1}, (\vartheta_{ie}^v)^{\beta_{i2}-1}, (\vartheta_{ie}^w)^{\beta_{i2}-1}\}$.

Inserting (45) into (44), one has

$$
\begin{aligned}
\dot{V} \le & \sum_{i=1}^N \Big(-c_{i0}'\|\boldsymbol{E}_i\|^2 - c_{i1}\|\boldsymbol{\zeta}_i\|^2 - c_{i2}\boldsymbol{\zeta}_i^T\boldsymbol{\iota}_{i\zeta}\boldsymbol{\zeta}_i - c_{i3}\|\boldsymbol{\vartheta}_{ie}\|^2 \\
& - c_{i4}\boldsymbol{\vartheta}_{ie}^T\boldsymbol{\iota}_{i\vartheta}\boldsymbol{\vartheta}_{ie} - c_{i5}'\|\tilde{\boldsymbol{W}}_i\|^2 + \varepsilon_i\ \Big) \\
\le & \sum_{i=1}^N \Big(-c_{i0}'\|\boldsymbol{E}_i\|^2 - c_{i1}'\|\boldsymbol{\zeta}_i\|^2 - c_{i3}'\|\boldsymbol{\vartheta}_{ie}\|^2 - c_{i5}'\|\tilde{\boldsymbol{W}}_i\|^2 + \varepsilon_i\ \Big),
\end{aligned}
\tag{46}
$$

where $c_{i1}' = c_{i1} + c_{i2}\underline{\lambda}(\boldsymbol{\iota}_{i\zeta})$ and $c_{i3}' = c_{i3} + c_{i4}\underline{\lambda}(\boldsymbol{\iota}_{i\vartheta})$.

Letting $c_1 = \min_{i=1,\ldots,N}\{c_{i0}', c_{i1}', c_{i3}', c_{i5}', c_{i6}'\}$ and $\varepsilon = \sum_{i=1}^N \varepsilon_i$, it devises that $\dot{V} \le -h_1 V + \varepsilon$ with $h_1 = 2c_1$. Therefore, all error signals of the closed-loop system are uniformly ultimately bounded for $|\zeta_{ik}| < \iota_{ik}$ and $|\vartheta_{ie}^l| < \iota_{il}$, $i = 1, \ldots, N, k = x, y, \psi$, and $l = u, v, w$.

Case 2. For $|\zeta_{ik}| \ge \iota_{ik}$ and $|\vartheta_{ie}^l| \ge \iota_{il}$, $i = 1, \ldots, N, k = x, y, \psi, l = u, v, w$, it gets

$$
\boldsymbol{\gamma}_i(\boldsymbol{\zeta}_i) = \text{sig}^{\beta_{i1}}(\boldsymbol{\zeta}_i) \quad \text{and} \quad \boldsymbol{\gamma}_i(\boldsymbol{\vartheta}_{ie}) = \text{sig}^{\beta_{i2}}(\boldsymbol{\vartheta}_{ie}).
\tag{47}
$$

Then, the derivative of V by (43) is represented as

$$
\begin{aligned}
\dot{V} \le \sum_{i=1}^N \Big(& -c_{i0}'\|\boldsymbol{E}_i\|^2 - c_{i1}\|\boldsymbol{\zeta}_i\|^2 - c_{i2}\|\boldsymbol{\zeta}_i\|^{\beta_{i1}+1} \\
& - c_{i3}\|\boldsymbol{\vartheta}_{ie}\|^2 - c_{i4}\|\boldsymbol{\vartheta}_{ie}\|^{\beta_{i2}+2} - c_{i5}'\|\tilde{\boldsymbol{W}}_i\|^2 + \varepsilon_i\ \Big).
\end{aligned}
\tag{48}
$$

From Lemma 2, the following inequalities are obtained

$$
\begin{aligned}
\|\boldsymbol{E}_i\|^2 &\ge \frac{1-\beta_{i3}}{2}\|\boldsymbol{E}_i\|^2 + \|\boldsymbol{E}_i\|^{\beta_{i3}+1} - \frac{1-\beta_{i3}}{2}, \\
\|\tilde{\boldsymbol{W}}_i\|^2 &\ge \frac{1-\beta_{i4}}{2}\|\tilde{\boldsymbol{W}}_i\|^2 + \|\tilde{\boldsymbol{W}}_i\|^{\beta_{i4}+1} - \frac{1-\beta_{i4}}{2},
\end{aligned}
\tag{49}
$$

where $0 < \beta_{i3}, \beta_{i4} < 1$.

Substituting (49) into (48), one has

$$
\begin{aligned}
\dot{V} \le \sum_{i=1}^N \Big(& -c_{i1}\|\boldsymbol{\zeta}_i\|^2 - c_{i2}\|\boldsymbol{\zeta}_i\|^{\beta_{i1}+1} - c_{i3}\|\boldsymbol{\vartheta}_{ie}\|^2 - c_{i4}\|\boldsymbol{\vartheta}_{ie}\|^{\beta_{i2}+2} \\
& - c_{i0}''\|\boldsymbol{E}_i\|^2 - c_{i0}'\|\boldsymbol{E}_i\|^{\beta_{i3}+1} - c_{i5}''\|\tilde{\boldsymbol{W}}_i\|^2 - c_{i5}'\|\tilde{\boldsymbol{W}}_i\|^{\beta_{i4}+1} + \varepsilon_i'\ \Big),
\end{aligned}
\tag{50}
$$

where $c_{i0}'' = c_{i0}'(1 - \beta_{i3})/2$, $c_{i5}'' = c_{i5}'(1 - \beta_{i4})/2$ and $\varepsilon_i' = \varepsilon_i + c_{i0}'' + c_{i5}''$.

Define $\boldsymbol{\zeta} = [\boldsymbol{\zeta}_1^T, \ldots, \boldsymbol{\zeta}_N^T]^T$, $\boldsymbol{\vartheta}_e = [\boldsymbol{\vartheta}_{1e}^T, \ldots, \boldsymbol{\vartheta}_{Ne}^T]^T$, $\boldsymbol{E} = [\boldsymbol{E}_1^T, \ldots, \boldsymbol{E}_N^T]^T$ and $\tilde{\boldsymbol{W}} = [\tilde{\boldsymbol{W}}_1^T, \ldots, \tilde{\boldsymbol{W}}_N^T]^T$. Then, the derivative of V can be represented as

$$
\begin{aligned}
\dot{V} \le & -c_2\left(\|\boldsymbol{\zeta}\|^2 + \|\boldsymbol{\vartheta}_e\|^2 + \|\boldsymbol{E}\|^2 + \|\tilde{\boldsymbol{W}}\|^2\right) - c_3\left(\|\boldsymbol{\zeta}\|^{\beta+1} \right. \\
& \left. + \|\boldsymbol{\vartheta}_e\|^{\beta+1} + \|\boldsymbol{E}\|^{\beta+1} + \|\tilde{\boldsymbol{W}}\|^{\beta+1}\right) + \varepsilon',
\end{aligned}
\tag{51}
$$

where $c_2 = \min_{i=1,\ldots,N}\{c_{i1}, c_{i3}, c_{i0}'', c_{i5}''\}$, $c_3 = \min_{i=1,\ldots,N}\{c_{i2}, c_{i4}, c_{i0}', c_{i5}'\}$, $\beta = \min_{i=1,\ldots,N}\{\beta_{i1}, \beta_{i2}, \beta_{i3}, \beta_{i4}\}$ and $\varepsilon' = \sum_{i=1}^N \varepsilon_i'$.

From Lemma 1, the following inequality can be obtained

$$
\dot{V} \le -h_2 V - h_3 V^{\frac{\beta+1}{2}} + \varepsilon',
\tag{52}
$$

where $h_2 = 2c_2$ and $h_3 = 2c_3$. Then, it deduces

$$
\dot{V} \le -(h_2 - \varepsilon'/V)V - h_3 V^{\frac{\beta+1}{2}}
\tag{53}
$$

and

$$
\dot{V} \le -h_2 V - (h_3 - \varepsilon'/V^{\frac{\beta+1}{2}})V^{\frac{\beta+1}{2}}.
\tag{54}
$$

When $V > \varepsilon'/h_2$ for the inequality (53), it gets

$$
\dot{V} \le -h_2' V - h_3' V^{\frac{\beta+1}{2}},
$$

where $h_2' = h_2 - \varepsilon'/V$ and $h_3' = h_3$. According to Lemma 3, V can arrive at the region $\{V \le \varepsilon'/h_2\}$ in the settling time T_1 satisfying

$$
T_1 = t_0 + \frac{2}{h_2'(1-\beta)}\ln\left(\frac{h_2'V^{\frac{1-\beta}{2}} + h_3'}{h_3'}\right).
$$

When $V > (\varepsilon'/h_3)^{2/(1+\beta)}$ for the inequality (54), it gets

$$
\dot{V} \le -h_2'' V - h_3'' V^{\frac{\beta+1}{2}},
$$

where $h_2'' = h_2$ and $h_3'' = h_3 - \varepsilon'/V^{\frac{\beta+1}{2}}$. According to Lemma 3, V can converge to the region $\{V \le (\varepsilon'/h_3)^{2/(1+\beta)}\}$ in the settling time T_2 satisfying

$$
T_2 = t_0 + \frac{2}{h_2''(1-\beta)}\ln\left(\frac{h_2''V^{\frac{1-\beta}{2}} + h_3''}{h_3''}\right).
$$

Thereby, it can be concluded that V can reach the set $\{V \le \min\{\varepsilon'/h_2, (\varepsilon'/h_3)^{2/(1+\beta)}\}\}$ within finite time $T^* = \max\{T_1, T_2\}$.

Remark 2. To facilitate the implementation of the proposed method, a basic adjustment guideline of relative parameters is summarized as follows:

(1) For TPPs, the selection of $\bar{\delta}_{ik}$, $\underline{\delta}_{ik}$, $\rho_{ik,0}$ ought to ensure that $-\underline{e}_{ik}(0) \le e_{ik} \le \bar{e}_{ik}(0), k = x, y, \psi$ holds from (17). The state-steady boundaries $\bar{\delta}_{ik}\rho_{ik,\infty}$ and $-\underline{\delta}_{ik}\rho_{ik,\infty}$ are decided by the equipped sensor. $\varkappa_{ik}$ is a vital parameter to adjust the convergence rate, which is determined by the actuator capability of ASVs in practice.

(2) For control laws and observer, the large gains are capable to achieve a faster error convergence. But the overlarge gains may lead to the poor output response. Accordingly, a trade-off should be recommended between convergence rate and stability.

5. Simulation results

In this section, we provide some simulation results with comparison analysis to manifest the effectiveness and superiority of proposed TPP method. All results are obtained by Matlab/Simulink with a fixed sampling frequency of 100 Hz.

In this simulation, we consider five ASVs named as ASV1∼ASV5 and one virtual leader named as ASV0, and Fig. 3 depicts their communication topology. We aim to achieve a body-fixed triangular formation

Table 1
Initial status of five ASVs.

Parameter	Value	Parameter	Value
$\boldsymbol{\eta}_1^T$	$[-67, -38, \pi/2]$	$\boldsymbol{P}_{1r}$	$\boldsymbol{R}_r[0, 0, 0]^T$
$\boldsymbol{\eta}_2^T$	$[-71, -44, \pi/2]$	$\boldsymbol{P}_{2r}$	$\boldsymbol{R}_r[-4, 4, 0]^T$
$\boldsymbol{\eta}_3^T$	$[-60, -37, \pi/2]$	$\boldsymbol{P}_{3r}$	$\boldsymbol{R}_r[-4, -4, 0]^T$
$\boldsymbol{\eta}_4^T$	$[-73, -48, 2\pi/3]$	$\boldsymbol{P}_{4r}$	$\boldsymbol{R}_r[-8, 8, 0]^T$
$\boldsymbol{\eta}_5^T$	$[-56, -35, 4\pi/5]$	$\boldsymbol{P}_{5r}$	$\boldsymbol{R}_r[-8, -8, 0]^T$

Fig. 3. The communication topology.

consisted of ASV1~ASV5. The Huangpu River is a river with a large shipping volume and a curved channel. Thus, we select it as an application scenario, as shown in the snapshot from Google Maps in Fig. 3. It is assumed that the virtual leader ASV0 sails along a predefined reference trajectory $\boldsymbol{\eta}_r(t) = [x_r(t), y_r(t), \psi_r(t)]^T = [-10 - t/8 + 80\cos(-t/320 + 5\pi/4), 20 + t/16 + 80\sin(-t/320 + 5\pi/4), \mathrm{atan2}(1/16 - 0.25\cos(-t/320 + 5\pi/4), 1/8 - 0.25\sin(-t/320 + 5\pi/4))]^T$. The model parameters of ASV1~ASV5 can be found in Fossen (2011). Without loss of generality, saturation parameters are set as $\bar{\tau}_{ia}^u = 15$ N, $\underline{\tau}_{ia}^u = -10$ N, $\bar{\tau}_{ia}^v = -\underline{\tau}_{ia}^v = 5$ N, and $\underline{\tau}_{ia}^w = -\bar{\tau}_{ia}^w = -8$ N m. According to (17) and (18), different initial errors lead to the different shapes of TPPs. To reflect the feature, the initial positions and headings of ASV1~ASV5 are set in Table 1. And the time-varying deviations of formation are also provided by Table 1 with

$$\boldsymbol{R}_r = \begin{bmatrix} \cos(\psi_r) & -\sin(\psi_r) & 0 \\ \sin(\psi_r) & \cos(\psi_r) & 0 \\ 0 & 0 & 1 \end{bmatrix}.$$

Guided by the policies in Remark 2, relative TPP parameters used in this simulation are set as Table 2. In addition, Table 2 also summaries the relative parameters of the AFSO (10), the C^1 finite-time guidance law (25), the finite-time command filter (28) and the C^1 finite-time saturated control law (30). Furthermore, some comparison results with traditional PPC (Dai et al., 2022a) are provided to illustrate the preeminence of the proposed TPP method.

Figs. 4–9 plot the simulation results. The comparison simulations are conducted with the reference trajectory $\boldsymbol{\eta}_r(t)$, the same communication topology, and initial position by using the PPC method from Dai et al. (2022a). Specifically, Fig. 4 depicts the actual trajectories of five ASVs and virtual leader ASV0 with snapshots at 0 s, 150 s, 300 s, 450 s and 600 s, respectively. It is seen that ASV1~ASV5 with the proposed TPP method achieve the desired distributed time-varying formation from different initial status, and all transient processes are smooth. In contrast to traditional PPC, the proposed method is able to avoid the undesired overshoot for a group of ASVs shown in Figs. 4 and 5. Fig. 5 plots the tracking errors of five ASVs based on the TPP

Table 2
Relative parameters of the proposed TPP method.

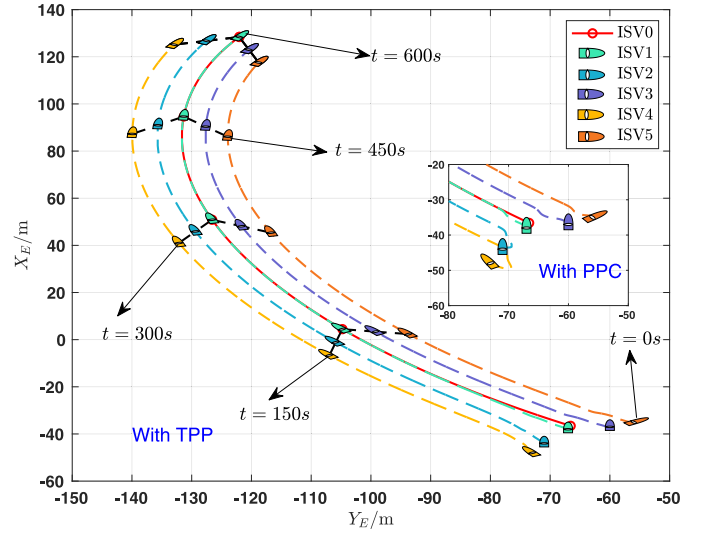| Parameter	Value	Parameter	Value
$\rho_{ix,0}$	2.5	$\rho_{iy,0}$	1.5
$\rho_{i\psi,0}$	0.8	$\rho_{ix,\infty}, \rho_{iy,\infty}$	0.1
$\rho_{i\psi,\infty}$	0.05	$\varkappa_{ik}$	0.05
$\bar{\delta}_{ik}(e_{ik,0} > 0)$	0.9	$\bar{\delta}_{ik}(e_{ik,0} < 0)$	0.6
$\underline{\delta}_{ik}(e_{ik,0} > 0)$	0.6	$\underline{\delta}_{ik}(e_{ik,0} < 0)$	0.9
$k_{i1,x}, k_{i1,y}$	0.4	$k_{i1,\psi}$	0.2
$k_{i2,k}$	0.1	$k_{i3,l}$	1.0
$k_{i4,l}$	1.0	ι_{ik}	0.001
ι_{il}	0.001	μ_{iu}	$1 - 0.6|\sin(t/50)|$
μ_{iv}	$1 - 0.4|\sin(t/100)|$	μ_{iw}	$1 - 0.2|\sin(t/50)|$
$\boldsymbol{L}_{i1}$	diag$\{20, 20, 20\}$	$\boldsymbol{L}_{i2}$	diag$\{100, 100, 100\}$
$\boldsymbol{L}_{i3}$	20	$\boldsymbol{L}_{i4}$	20

Fig. 4. The formation trajectories of ASV1~ASV5 based on the proposed TPP method and the PPC method (Dai et al., 2022a).

method by using the saturated inputs and unconstrained inputs. From sub Fig. 5-(a) to -(c), unconstrained control inputs can make tracking errors from different initial values converge to the same position within 15 s. Affected by saturation property, all tracking errors fluctuate in the transient state, but still converge to the prescribed spaces defined as (18) without any transient overshoots, i.e., formation control objective (7) is achieved. According to Fig. 5-(a), it is found that errors e_{1x} and e_{3x} first increase and then decrease due to two reasons. One is that the initial value $\bar{e}_{ix}(0)$ of the constraint boundary is too large owing to the selection of $\rho_{ix,0}$ and $\bar{\delta}_{ix}$, and the other is the saturation characteristics of the ASV's actuator. The fluctuation of e_{5x} is mainly caused by the actuator saturation. Fig. 5-(b) to -(c) are similar to Fig. 5-(a). Fig. 6 shows the partial tracking errors of ASV4 by using the PPC method. Compared with PPC constraints, the proposed TPP constraints have the more tight space. And their bounds are on the same side of origin, which restricts tracking errors from converging to 0 across boundaries. However, the boundaries of PPC are distributed on both sides of the origin, which allows the overshoot of tracking errors. Fig. 7 displays the estimation performance for the surge, sway and yaw velocity by using the proposed AFSO (10). It is observed that there are fluctuations after all velocities converge to steady states, which is because control signals τ_{ia} cannot fully work due to the effectiveness parameter $\mu_i(0, t)$. Fig. 8 draws that the proposed FLS (9) is able to estimated the unknown disturbances from internal uncertainties and external disturbances from winds, waves, and currents. Fig. 9 describes
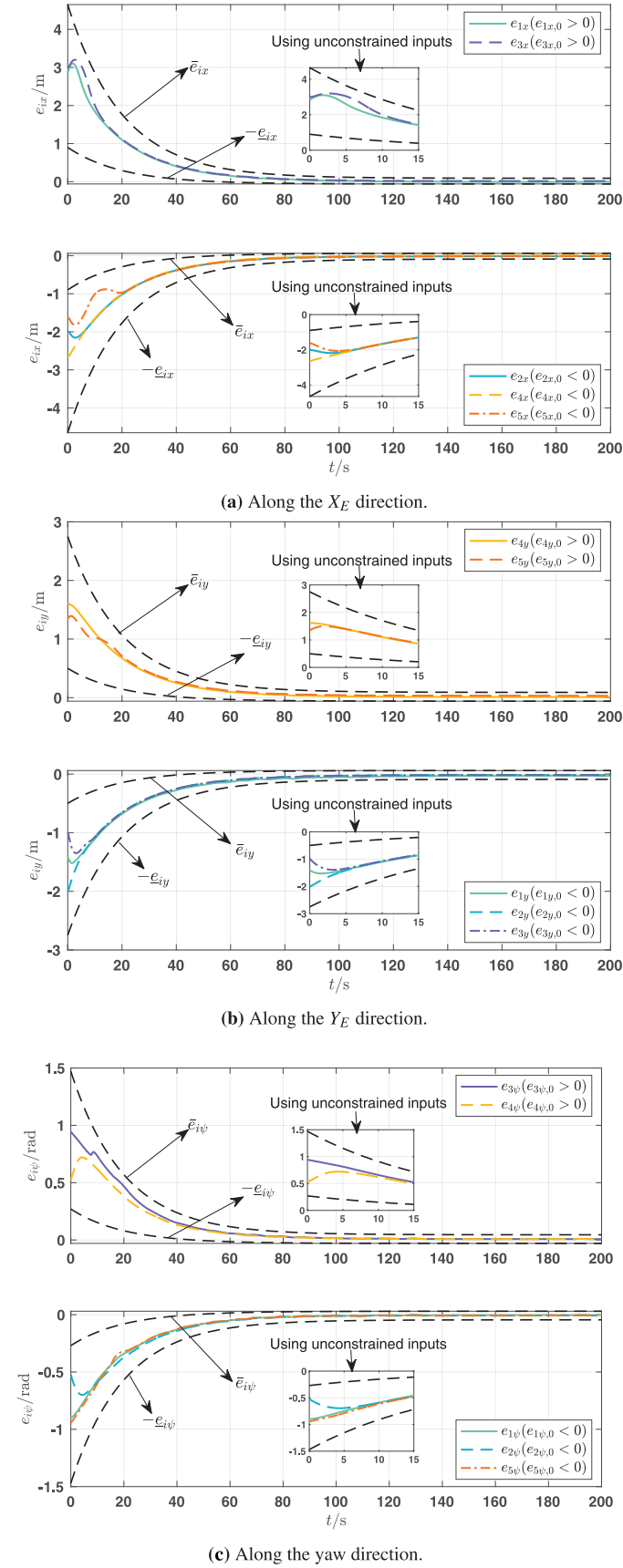
(a) Along the X_E direction.

(b) Along the Y_E direction.

(c) Along the yaw direction.

Fig. 5. The earth-fixed tracking errors based on proposed TPP method (by using saturated inputs and unconstrained inputs).
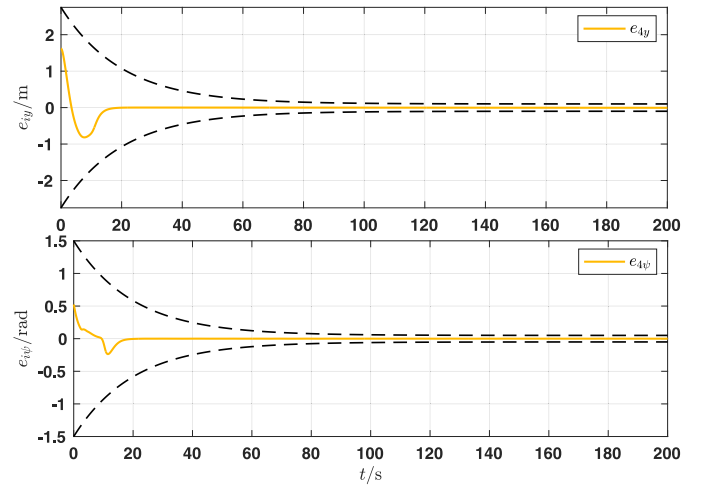

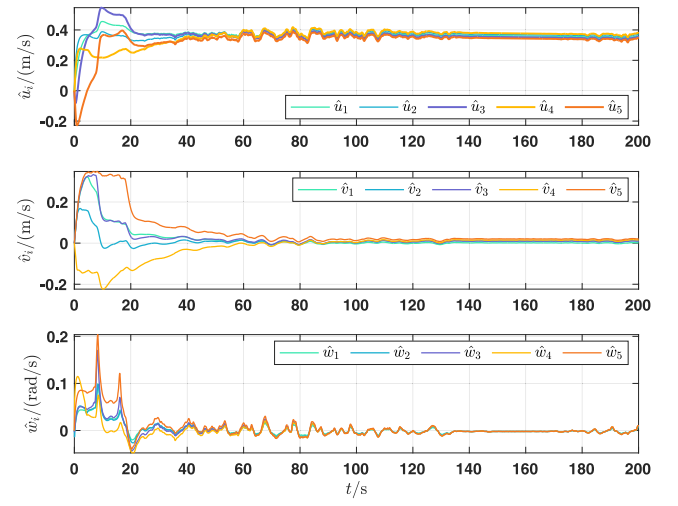**Fig. 6.** Tracking errors of ASV4 based on the PPC method.

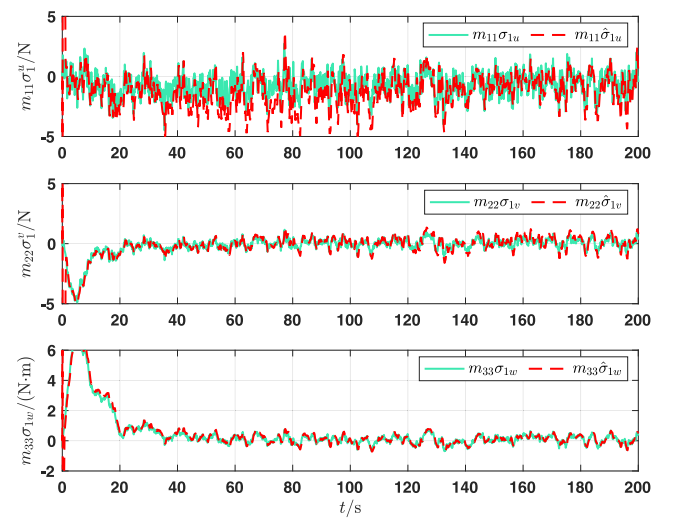**Fig. 7.** The estimated velocities in $X_B - Y_B$ reference frame.

Fig. 8. The estimated disturbances.

the saturated surge, sway forces and yaw moments of ASV1~ASV5 without violating the saturation constraints (see Fig. 5).
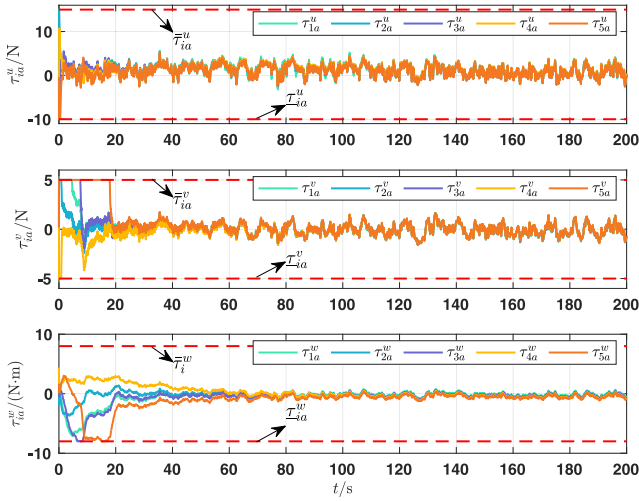
Fig. 9. The control forces and moments of five follower ASVs.

6. Conclusion

This paper investigates a trajectory-guided performance-prescribed time-varying formation problem of multiple ASVs only with the measurable position and heading information. Each ASV suffers from input saturations, model uncertainties, and external disturbances. A distributed finite-time performance-prescribed time-varying formation control method is proposed for ASVs based on AFSO. With the proposed AFSO, the unavailable velocities and unknown disturbances are able to be precisely recovered. By utilizing the constructed smooth switch functions, the proposed finite-time formation guidance law can be ensured to be continue and differentiable. With the TPP-based guidance law, the distributed time-varying formation of multiple ASVs is achieved and the tracking errors evolved within TPP constraints regardless of input saturations. The finite-time command filter is used to smooth the guidance signals from the kinetic level. Based on the estimated velocities and disturbances, the finite-time saturated control law is developed to track the guidance signals within finite time. Finally, simulation results demonstrate the feasibility and effectiveness of the proposed method.

CRediT authorship contribution statement

Wentao Wu: Software, Validation, Writing – original draft, Visualization, Writing – review & editing, Data curation, Project administration. **Yibo Zhang:** Supervision, Conceptualization, Funding acquisition, Project administration, Methodology, Investigation. **Weidong Zhang:** Supervision, Methodology, Investigation, Resources, Project administration, Funding acquisition, Project administration. **Wei Xie:** Methodology, Investigation.

Declaration of competing interest

The authors declare that they have no known competing financial interests or personal relationships that could have appeared to influence the work reported in this paper.

Data availability

The data that has been used is confidential.

References

Chen, L., Cui, R., Yang, C., Yan, W., 2020. Adaptive neural network control of underactuated surface vessels with guaranteed transient performance: Theory and experimental results. IEEE Trans. Ind. Electron. 67 (5), 4024–4035.

Dai, S.-L., He, S., Cai, H., Yang, C., 2022a. Adaptive leader–follower formation control of underactuated surface vehicles with guaranteed performance. IEEE Trans. Syst. Man, Cybern., Syst. 52 (3), 1997–2008.

Dai, S.-L., He, S., Lin, H., Wang, C., 2018. Platoon formation control with prescribed performance guarantees for USVs. IEEE Trans. Ind. Electron. 65 (5), 4237–4246.

Dai, S.-L., He, S., Ma, Y., Yuan, C., 2022b. Cooperative learning-based formation control of autonomous marine surface vessels with prescribed performance. IEEE Trans. Syst. Man, Cybern., Syst. 52 (4), 2565–2577.

Dai, S.-L., Wang, M., Wang, C., 2015. Neural learning control of marine surface vessels with guaranteed transient tracking performance. IEEE Trans. Ind. Electron. 63 (3), 1717–1727.

Du, B., Lin, B., Zhang, C., Dong, B., Zhang, W., 2022. Safe deep reinforcement learning-based adaptive control for USV interception mission. Ocean Eng. 246, 110477.

Fossen, T.I., 2011. Handbook of Marine Craft Hydrodynamics and Motion Control. John Wiley & Sons.

Gao, S., Peng, Z., Wang, H., Liu, L., Wang, D., 2022. Safety-critical model-free control for multi-target tracking of USVs with collision avoidance. IEEE/CAA J. Autom. Sinica 9 (7), 1323–1326.

Gu, N., Peng, Z., Wang, D., Shi, Y., Wang, T., 2019. Antidisturbance coordinated path following control of robotic autonomous surface vehicles: Theory and experiment. IEEE/ASME Trans. Mechatron. 24 (5), 2386–2396.

Gu, N., Wang, D., Peng, Z., Liu, L., 2019. Observer-based finite-time control for distributed path maneuvering of underactuated unmanned surface vehicles with collision avoidance and connectivity preservation. IEEE Trans. Syst. Man, Cybern., Syst. 51 (8), 5105–5115.

He, S., Wang, M., Dai, S., Luo, F., 2019. Leader-follower formation control of USVs with prescribed performance and collision avoidance. IEEE Trans. Ind. Inf. 15 (1), 572–581.

Ji, R., Yang, B., Ma, J., Ge, S.S., 2021. Saturation-tolerant prescribed control for a class of mimo nonlinear systems. IEEE Trans. Cybern. 1–15. http://dx.doi.org/10.1109/TCYB.2021.3096939.

Jia, Z., Hu, Z., Zhang, W., 2019. Adaptive output-feedback control with prescribed performance for trajectory tracking of underactuated surface vessels. ISA Trans. 95, 18–26.

Levant, A., 1998. Robust exact differentiation via sliding mode technique. Automatica 34 (3), 379–384.

Li, M., Guo, C., Yu, H., 2021. Global finite-time control for coordinated path following of multiple underactuated unmanned surface vehicles along one curve under directed topologies. Ocean Eng. 237, 109608.

Li, M., Guo, C., Yu, H., Yuan, Y., 2022b. Event-triggered containment control of networked underactuated unmanned surface vehicles with finite-time convergence. Ocean Eng. 246, 110548.

Li, M., Li, T., Gao, X., Shan, Q., Chen, C.P., Xiao, Y., 2020. Adaptive NN event-triggered control for path following of underactuated vessels with finite-time convergence. Neurocomputing 379, 203–213.

Li, J., Xiang, X., Yang, S., 2022a. Robust adaptive neural network control for dynamic positioning of marine vessels with prescribed performance under model uncertainties and input saturation. Neurocomputing 484, 1–12. http://dx.doi.org/10.1016/j.neucom.2021.03.136.

Li, T., Zhao, R., Chen, C.L.P., Fang, L., Liu, C., 2018. Finite-time formation control of under-actuated ships using nonlinear sliding mode control. IEEE Trans. Cybern. 48 (11), 3243–3253.

Lu, Y., Xu, X., Qiao, L., Zhang, W., 2021. Robust adaptive formation tracking of autonomous surface vehicles with guaranteed performance and actuator faults. Ocean Eng. 237, 109592. http://dx.doi.org/10.1016/j.oceaneng.2021.109592.

Park, B.S., Yoo, S.J., 2019. An error transformation approach for connectivity-preserving and collision-avoiding formation tracking of networked uncertain underactuated surface vessels. IEEE Trans. Cybern. 49 (8), 2955–2966.

Peng, Z., Gu, N., Zhang, Y., Liu, Y., Wang, D., Liu, L., 2019. Path-guided time-varying formation control with collision avoidance and connectivity preservation of underactuated autonomous surface vehicles subject to unknown input gains. Ocean Eng. 191, 106501.

Peng, Z., Wang, J., Wang, D., Han, Q., 2021. An overview of recent advances in coordinated control of multiple autonomous surface vehicles. IEEE Trans. Ind. Inf. 17 (2), 732–745.

Qian, C., Lin, W., 2001. A continuous feedback approach to global strong stabilization of nonlinear systems. IEEE Trans. Automat. Control 46 (7), 1061–1079.

Shi, Y., Shen, C., Fang, H., Li, H., 2017. Advanced control in marine mechatronic systems: A survey. IEEE/ASME Trans. Mechatron. 22 (3), 1121–1131.

Wang, L.-X., 1994. Adaptive Fuzzy Systems and Control: Design and Stability Analysis. Prentice-Hall, Inc..

Wang, N., Gao, Y., Zhang, X., 2021b. Data-driven performance-prescribed reinforcement learning control of an unmanned surface vehicle. IEEE Trans. Neural Netw. Learn. Syst. 32 (12), 5456–5467.

Wang, N., Karimi, H.R., Li, H., Su, S.-F., 2019. Accurate trajectory tracking of disturbed surface vehicles: A finite-time control approach. IEEE/ASME Trans. Mechatron. 24 (3), 1064–1074.

Wang, H., Li, M., Zhang, C., Shao, X., 2021a. Event-based prescribed performance control for dynamic positioning vessels. IEEE Trans. Circuits Syst. II: Express Briefs 68 (7), 2548–2552.

Wu, W., Peng, Z., Liu, L., Wang, D., 2022a. A general safety-certified cooperative control architecture for interconnected intelligent surface vehicles with applications to vessel train. IEEE Trans. Intell. Veh. http://dx.doi.org/10.1109/TIV.2022.3168974.

Wu, W., Peng, Z., Wang, D., Liu, L., Gu, N., 2022b. Anti-disturbance leader–follower synchronization control of marine vessels for underway replenishment based on robust exact differentiators. Ocean Eng. 248, 110686.

Wu, W., Peng, Z., Wang, D., Liu, L., Han, Q.-L., 2022c. Network-based line-of-sight path tracking of underactuated unmanned surface vehicles with experiment results. IEEE Trans. Cybern. 52 (10), 10937–10947.

Wu, W., Zhang, Y., Zhang, W., Xie, W., 2022d. Output-feedback finite-time safety-critical coordinated control of path-guided marine surface vessels based on neurodynamic optimization. IEEE Trans. Syst. Man, Cybern., Syst. 1–13. http://dx.doi.org/10.1109/TSMC.2022.3205637.

Yu, C., Liu, C., Lian, L., Xiang, X., Zeng, Z., 2019. ELOS-based path following control for underactuated surface vehicles with actuator dynamics. Ocean Eng. 187, 106139.

Yu, S., Yu, X., Shirinzadeh, B., Man, Z., 2005. Continuous finite-time control for robotic manipulators with terminal sliding mode. Automatica 41 (11), 1957–1964.

Zhang, J.-X., Chai, T., 2021. Singularity-free continuous adaptive control of uncertain underactuated surface vessels with prescribed performance. IEEE Trans. Syst. Man, Cybern., Syst. 1–10. http://dx.doi.org/10.1109/TSMC.2021.3129798.

Zhang, Y., Wang, D., Yin, Y., Peng, Z., 2021b. Event-triggered distributed coordinated control of networked autonomous surface vehicles subject to fully unknown kinetics via concurrent-learning-based neural predictor. Ocean Eng. 234, 108966.

Zhang, J., Xiang, X., Li, W., 2021a. Advances in marine intelligent electromagnetic detection system, technology and applications: A review. IEEE Sens. J..

Zhang, J.-X., Yang, G.-H., 2018. Fault-tolerant leader-follower formation control of marine surface vessels with unknown dynamics and actuator faults. Int. J. Robust Nonlinear Control 28 (14), 4188–4208.

Zhu, G., Ma, Y., Li, Z., Malekian, R., Sotelo, M., 2021. Adaptive neural output feedback control for MSVs with predefined performance. IEEE Trans. Veh. Technol. 70 (4), 2994–3006.